Lab on a Chip

Accepted Manuscript

ROYAL SOCIETY OF CHEMISTRY

www.rsc.org/loc

Continuous flow micro-bioreactors for the production of biopharmaceuticals: effect of geometry, surface texture, and flow rate

Table of content entry

(Alvarez et al., 2014).

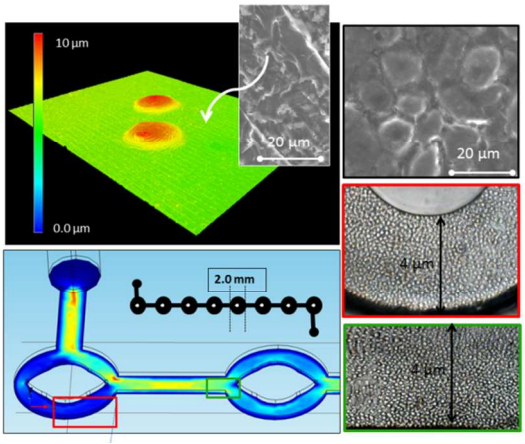

Continuous flow micro-devices, used as bioreactors for the culture of attached recombinant CHO cells, produce monoclonal antibodies at high productivities.

Cite this: DOI: 10.1039/c0xx00000x

www.rsc.org/xxxxxx

PAPER

Continuous flow micro-bioreactors for the production of biopharmaceuticals: effect of geometry, surface texture, and flow rate

Lucía D. Garza-García[a], Erika García-López[c], Sergio Camacho-León[b], María del Refugio Rocha-Pizaña[a], Felipe López-Pacheco[a], Julián López-Meza[a], Diana Araiz-Hernández [a], Eduardo J. Tapia-Mejía[b], Grissel Trujillo-de Santiago[a], Ciro A. Rodríguez-González[c], and Mario Moisés Alvarez[*a]

Received (in XXX, XXX) Xth XXXXXXXXX 20XX, Accepted Xth XXXXXXXXX 20XX

DOI: 10.1039/b000000x

We used continuous flow micro-devices as bioreactors for the production of a glycosylated pharmaceutical product (a monoclonal antibody). We cultured CHO cells on the surface of PMMA/PDMS micro-channels that had been textured by micromachining and coated with fibronectin. Three different micro-channel geometries (a wavy channel, a zigzag channel, and a series of donut-shape reservoirs) were tested in a continuous flow regime in the range of 3 to 6 µL min^{-1}. Both the geometry of the micro-device and the flow rate had a significant effect on cell adhesion, cell proliferation, and monoclonal antibody production. The most efficient configuration was a series of donut-shaped reservoirs, which yielded mAb concentrations of 7.2 mg L^{-1} at residence times lower than one minute and steady-state productivities above 9 mg mL^{-1} min^{-1}. These rates are at about 3 orders of magnitude higher than that those observed in suspended-cell, stirred tank, fed-batch bioreactors.

Introduction

The production of biotherapeutics continues to grow in the pharmaceutical market. In 2011, the value of recombinant therapeutic protein production was estimated at $56 billion dollars and this is projected to be above $80 billion dollars by 2015 [1-3]. The most promising segment in terms of therapeutic and economic value is the production of monoclonal antibodies (mAbs) [3-6]. At present, commercial production of mAbs and other bio-therapeutics typically relies on synthesis by mammalian cell cultures suspended in 10 to 20 m^3 instrumented stirred tank bioreactors that are operated in fed-batch or (less frequently) perfusion modes [7-9]. Chinese Hamster Ovary (CHO) cells are the standard mammalian host for the production of proteins of pharmaceutical interest [10-12].

Fed-batch systems can support cell densities of between $5x10^6$ and $1x10^7$ cells mL^{-1}. Increases in cell density and, as a consequence, protein production can be obtained by using a perfusion system, where cells are maintained inside the tank and the product stream is removed at a controlled flow rate. Under this strategy, cell concentrations in the range of $1–6x10^7$ cells mL^{-1} can be achieved [12].

Although relatively well established, mAb production in stirred tanks still faces challenges related to process and product quality (*i.e.*, the demand for higher productivities, control of the glycosylation patterns of the product, process reproducibility, and process control) [7,8,13]. Most of these challenges are related to the high spatial and temporal variability of the conditions intrinsic to stirred tanks, and could be addressed by strategies aimed at more rigid control of the cell environment [13,14]. New market pressures, such as competition from biosimilars, will also oblige manufacturers to develop technology alternatives for highly flexible and cost-effective mAb manufacturing [12]. In addition, lab scale applications associated with the screening of process conditions for the production of biopharmaceuticals (*i.e.*, media formulation or optimization, selection of culture high-producer clones) will certainly benefit from a stricter control of the cell microenvironment [7].

Conceptually, one way to improve control is to reduce the relevant length scales of the system; for example, through miniaturization [15] in the form of micro-devices. In biological applications, a micro-device offers several benefits, including shorter response time, high surface/volume ratio (with important implications for the control of transfer phenomena), and a generally more homogeneous and controllable microenvironment [12,16]. A substantial number of experimental reports and reviews are now available on the use of micro-devices in a wide variety of cell culture applications. Recently published examples include the enrichment of cancer stem cells in PDMS micro-devices [17], the evaluation of toxicity of compounds in organ-on-a-chip systems [18,19], the use of high gas-liquid interface PDMS micro-chambers to enhance oxygen transfer to mammalian cells under static culture [20], and a microfluidic co-culture system (for normal and cancerous cells) for the investigation of bacterial cancer targeting [21] and for the study of complex integrated organ-level responses to bacteria and inflammatory cytokines [22]. A few notable examples of continuous flow micro-devices for cell culture have been published recently [18,23-27]. However, reports on the use of micro-devices for the production of recombinant proteins are still scarce [28,29]. To our knowledge, no report (other than our own previous communication [30]) has shown the effectiveness of micro-devices for the continuous production of biopharmaceuticals.

The application of a perfusion system within a micro-device for cell culture requires that the cells form strong attachments to the device surface. CHO cell lines can grow in anchorage dependent conditions when they are cultured in media containing fetal bovine serum (FBS). However, for industrial applications, CHO cell lines must be adapted to grow in suspension in chemically defined (*i.e.*, FBS-free) media. Consequently, CHO cell lines adapted for suspension culture do not form attachments to surfaces. However, our previous contribution [30] clearly demonstrated proof of concept for the use of continuous flow micro-devices for cell attachment and the production of a monoclonal antibody. In the present paper, we expand on this concept by providing additional support derived from experiments using three different micro-device systems (Figure 1) and different flow rates (in the range of 3 to 6 μL min^{-1}). We show that the geometry of the device and the flow rate play a key role in the performance of these continuous flow micro-bioreactors. We study the application of micro-devices built on either PMMA (polymethyl methacrylate) or PDMS (polydimethyl siloxane) – two commonly used polymers for micro-fluidic bioapplications [31-33] – for the production of a high-value recombinant therapeutic protein in attached CHO cell cultures. A biosimilar of Infliximab® was chosen as our model, as this biotherapeutic is a widely used monoclonal antibody for the treatment of inflammatory diseases.

The selection of the construction materials followed a simple rationale: PMMA and PDMS are non-toxic to cells, inexpensive, and amenable to micro-device construction. Cell cultures grown on PMMA/PDMS surfaces exhibit a high viability [33] and other relevant cell growth characteristics that are comparable to those observed in several of their counterparts [22, 24-29]. The body of our micro-devices was constructed of PMMA to facilitate micromachining, and the lid was made of PDMS to support appropriate oxygen mass transfer.

Materials and methods

Cells, culture media, and culture conditions

A CHO-S cell line (Invitrogen, Carlsbad, CA, USA) was genetically modified to generate a CHO-S clone, producer of a bio-similar of the monoclonal antibody Infliximab [34]. The cell culture medium consisted of a mixture of CD OPTICHO™ (Invitrogen, Carlsbad, CA, USA) and CHO CD EfficientFeed™ B (Invitrogen, Carlsbad, CA, USA) supplemented with 200 mM L-glutamine (Invitrogen, Carlsbad, CA, USA).

Suspension culture in fed-batch bioreactors

For comparison purposes, we conducted a series of three experiments in fully instrumented bioreactors (EZ-Control system from Applikon™, Netherlands) operated in fed-batch mode. For these experiments, we followed a protocol of 17 days of culture, seeding $2x10^5$ cells mL^{-1} in an initial volume of 1.0 L of CD OPTICHO™ cell culture medium supplemented with 200 mM L-glutamine. The reactor was supplemented by additions of 150 mL of CHO CD EfficientFeed™ B administered at days 1, 3, 5, 7, 9, and 11, and 13 of culture.

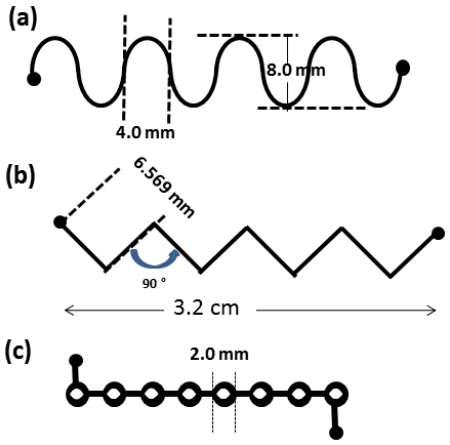

Figure 1. Different micro-device designs were used: (a) a wavy channel (WV); (b) a zigzag channel (ZZ); and (c) a serial-donut system (SD).

Microfluidic device fabrication

Three different micro-device geometries were built: a wavy channel (WV), a zigzag channel (ZZ), and a serial-donut channel (SD) device (Figure 1). The micro-devices were designed in CAD-CAM. The lower section of each micro-device, which consisted of PMMA, contained the micro-channel pattern. Micro-channels were fabricated by mechanically micromachining rectangular PMMA wafers (6 mm wide) [35] using a vertical milling machine (MAKINO F3, MF-70 Proxxon, CA, USA). A micro end milling tool (SGS39216) with a 0.410 μm cutting diameter was used.

Two different parameter settings were used to obtain different surface qualities in the bottom of the channels. Increasing the spindle speed to 11,000 RPM and decreasing the feed per tooth to 0.005 mm/tooth resulted in a micro-channel bottom surface with low roughness (LRS). The spindle speed was adjusted to 5,000 RPM, and feed per tooth to 0.015 mm/tooth, to produce a surface with an enhanced roughness (ERS) (approximately three times rougher).

The length of each micro-channel varied according to the geometry: 34 mm for WV; 44 mm for ZZ, and 28.9 mm for SD. Regardless of geometry, the width (0.5 mm), depth (0.1 mm), and diameter reservoir (1 mm) were the same for all micro-channels.

The micro-channels were covered with a rectangular PDMS wafer (3 mm wide). PDMS and the curing agent (Sylgard 184, Dow Corning Corp., Midland, MI, USA) were mixed with a 10:1 weight ratio. A mask with the same 2D dimensions as the PMMA layer was used to obtain the PDMS wafer. The PDMS was poured into the mask, cured at 121°C for 15 min, and then peeled from the mask. Reservoirs were generated in PDMS wafer with a sharpened blunt-tip needle. The PMMA and PDMS layers were thermally bonded by applying liquid PDMS around the borders and curing the resultant micro-device at 120°C for 20 min. Subsequently, hoses were bonded to the reservoirs following the same procedure. The micro-fluidic devices were used 24 h after being manufactured.

Before cell culture inoculation, the micro-channel surface was coated with fibronectin (FN) (20 μg mL^{-1}).

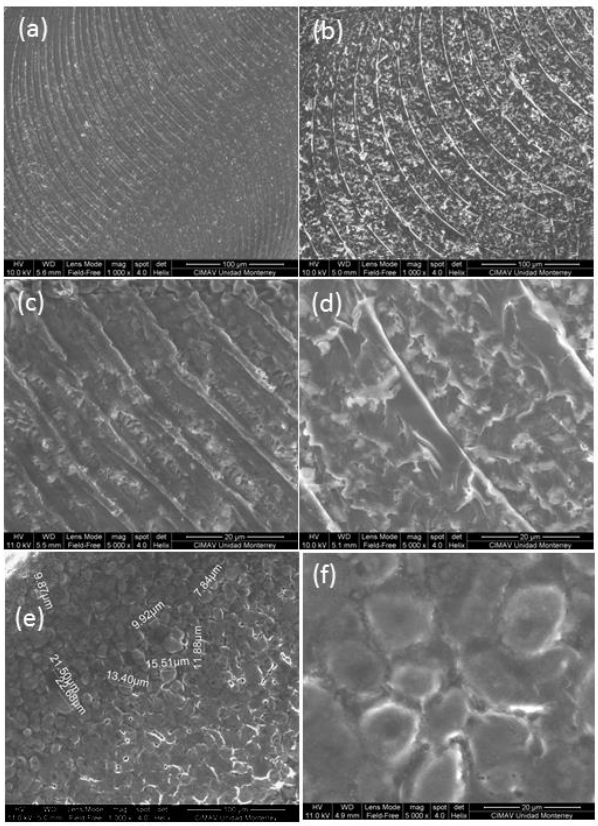

Figure 2. SEM micrographs of a low roughness surface at two different magnifications (a) 1000X and (c) 5000X; and an enhanced roughness surface without cells at (b) 1000X and (d) 5000X. SEM images of cells anchored to an enhanced roughness surface treated with fibronectin observed 48 h after continuous perfusion at two different magnifications (e) 1000X, and (f) 5000X.

Surface characterization

Low vacuum Scanning Electron Microscopy (SEM) was used to characterize both the low and enhanced roughness surfaces at different magnifications (1000X and 5000X). Additional SEM images of surfaces with confluent cell attachment were obtained (Figure 2). The roughness of the bottom surfaces of the micro-devices was also measured using a 3D non-contact optical profilometer (Axio CSM 700, Carl Zeiss, Oberkochen, Germany). The average roughness (Ra), the mean height of peaks (Rc) and the average spacing between two consecutive peaks or valleys (Rsm) were randomly determined at three different locations on the low and enhanced roughness surfaces using ISO 4287. A computer simulation of the surface topography (in Figure 3a and 3b) was performed using the software provided by the manufacturer.

Continuous micro-reactor experimental set-up

A Harvard 33 twin syringe pump (Harvard Apparatus, Inc., Holliston, MA, USA) was used to inject solutions, including the cell culture inoculation and continuous perfusion medium, into the micro-fluidic device. Sterilization of the micro-devices consisted of autoclaving at 120°C for 20 min, and subsequently introducing 70% ethanol at 10 µL min^{-1} under UV light for 30 min. Prior to cell inoculation, the micro-channel surface was coated with FN (Invitrogen, Carlsbad, CA, USA), the solution was introduced at 10 µL min^{-1} for 20 min, and the micro-device was incubated at 37°C for 1 h. Subsequently, the micro-channel was rinsed with sterile phosphate-buffered saline (PBS; Invitrogen, Carlsbad, CA, USA) at 10 µL min^{-1} for 30 min. Finally, a culture medium consisting of a mixture of CD OptiCHO™ and CHO CD EfficientFeed™ B was dispensed into the micro-channel. A viable cell density of $2x10^6$ cells min^{-1} was then introduced into each micro-device at 5 µL min^{-1}.

Cell culture in the micro-devices was divided into two stages. The first stage consisted of micro-device incubation at static conditions for 96 h at 33°C in an incubator with a humidified 8% CO_2 atmosphere. The second stage consisted of continuous injection feeding of the culture medium mixture into the micro-device for 48 h. The medium mixture was delivered at three different flow rates, namely 3, 5, and 6 µL min^{-1}. During the perfusion, the micro-devices and syringe pump were maintained inside an incubator at 31°C with a humidified 8% CO_2 atmosphere. Every day, pictures were taken with a Carl Zeiss 200 inverted fluorescence video microscope (Carl Zeiss, Jena, Germany) equipped with a 20X microscope objective.

Samples were collected at the system outlet after 96 h (at the end of the static incubation stage), and every 12 h during continuous perfusion.

Flow field characterization by CFD

Computational Fluid Dynamics (CFD) was used to simulate the velocity, shear stress, and vorticity fields within the three micro-device designs when operated under continuous flow at 3 and 5µL min^{1}. Briefly, the Comsol® software was used to model the internal geometry of each micro-device, and a user-controlled mesh calibrated for fluid dynamics was produced to fill the volume to be occupied by fluid. The meshes of the WV, ZZ, and SD systems were composed of 74,520; 212,720; and 57,494 domain elements, respectively. At each node of these meshes, the Navier Stokes equations were solved numerically to determine the local flow velocity in the laminar regime, using a non-slip condition at the channel boundaries. The density and viscosity of the cell culture medium mixture were estimated at 0.96 g mL^{-1} and 0.89 cP, respectively. The values of the velocity field were then used to calculate the local shear stresses and vorticities.

Cell attachment and proliferation

Cell proliferation was measured by analysis of optical microscopy images taken at different positions along the micro-channels, and under the different operational conditions. Each image was divided into quadrants, and the number of cells anchored in each quadrant was inspected using open source image analysis software (Image J, NIH). The areas of the individual cells were calculated and summed to estimate the area covered by cells at each quadrant. The ratio between the area covered by cells and the total area of the quadrant was used as an estimator of the extent of cell attachment.

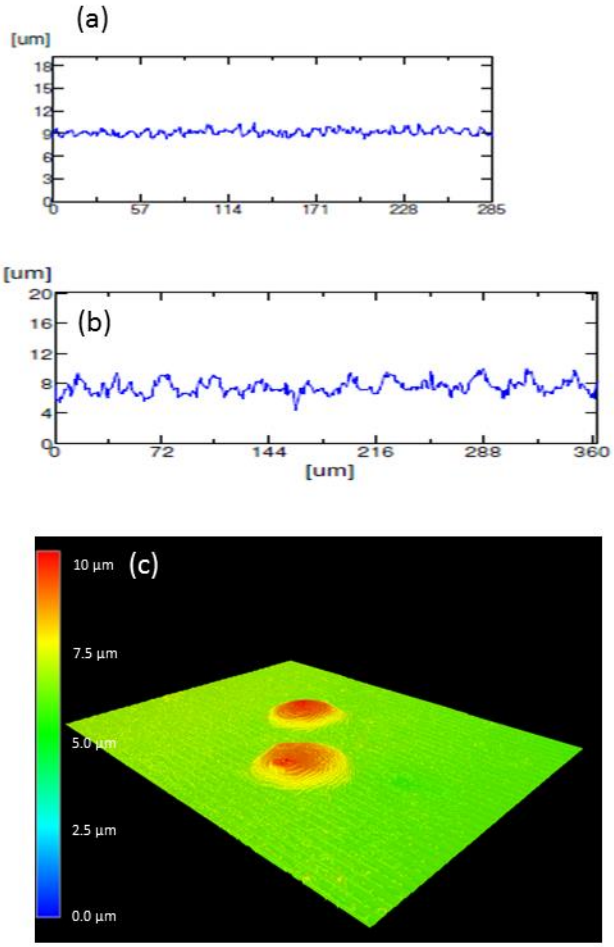

Figure 3. Profiles of samples with (a) low (LRS) and (b) enhanced roughness surfaces (ERS), as determined by confocal microscopy. (c) Topography of two cells anchored to an enhanced roughness surface coated with fibronectin as depicted by a confocal microscopy analysis.

mAb quantification

An enzyme-linked immunoabsorbent assay (ELISA) was used to quantify the monoclonal antibody samples as previously described [35]. Briefly, 100 µL well^{-1} of antigen (TNF-α at 5 µg L^{-1} from BioSource^{TM}; Invitrogen, Carlsbad, CA, USA) were added to 96-well plates. After an overnight incubation at room temperature, the antigen was removed and the plates were washed with PBC-Tween 0.05% and PBS. Subsequently, a blocking buffer (Pierce, N502, Rockford, IL, USA) was added to the plates, which were then incubated for 1 h and washed again. Samples with mAb were diluted in PBS, added at 100 µL well^{-1}, and plates were incubated for 1 h at room temperature. Afterwards, 100 µL well^{-1} of anti-human IgG Fc-HRP conjugate (Pierce, No. Cat. 31413, Rockford, IL, USA) were added at a 1:120,000 dilution and incubated for 1 h at room temperature. TMB substrate (Pierce, N301, Rockford, IL, USA) was then added at 100 µL well^{-1}, and plates were incubated for 15 min in the dark at room temperature. The reaction was stopped by addition of 1 M H_2SO_4 at 50 µL well^{-1}. The plates were read at 450 nm (OD_{450}) in a microwell reader (Biotek, Winooski, VA, USA).

Results and Discussion

Surface design and cell attachment

The microfabrication method we used for our micro-devices allowed us to impart different textures to the PMMA micro-channel surfaces. In preliminary experiments (not shown), we were unable to sustain cell attachment under flow conditions (in the range of 1 to 5 µL min^{-1}) on the low surface roughness (see Materials and Methods) surfaces of straight micro-channels. To increase cell adhesion, the surfaces of all micro-devices were micro-machined using different parameters to enhance the roughness. Our intention was to impart a rugosity of about the same order of magnitude as the size of a CHO cell (≈15 ± 10 µm). We characterized the low and enhanced roughness surfaces (LRS and ERS) using scanning electronic and confocal microscopy. Figure 2a-d compares electron microscope images (FEI Nova NanoSEM 200, Hillsboro, OR, USA) at two different magnifications for both types of micro-channel surface.

We used confocal microscopy to analyze the texture of the low and enhanced roughness surfaces (see Figure 3a and 3b). The average roughness (Ra), the mean height (Rc), and the average spacing (Rsm) were at least 1.7 fold higher in the enhanced roughness surface than in the low roughness surface (Table 1).

Table 1. Average roughness (Ra), mean height of peaks (Rc), and average spacing between two consecutive peaks or valleys (Rsm) for low (LRS) and enhanced roughness (ERS) micro-machined PMMA surfaces, as calculated by confocal microscopy.

Parameter	ERS (µm)	LRS (µm)
Ra	0.253 ± 0.035*	0.653 ± 0.102**
Rc	1.107 ± 0.094	2.609 ± 0.576
Rsm	10.030 ± 1.498	17.750 ± 2.079

* Standard deviation from two measures sampling a linear distance of 300 µm, and
** standard deviation from four measures sampling a linear distance of 300 µm.

Although the difference in rugosity and spacing parameters between the two qualities of the surface seems modest, this texturing most likely enhanced the adherence of cells simply by increasing the effective surface area available for attachment. The increased cell attachment observed in the ERS may be also attributed, at least partially, to a change in wettability (a parameter related to surface hydrophobicity and evaluated by measuring the contact angle between a surface and a drop of liquid). The correlation between average rugosity and wettability has recently been studied for several surfaces, including PMMA [36,37]. In the range of Ra values calculated for our micro-machined surfaces, an increase in roughness is associated with a discreet increment in wettability (a decrease of 8 to10 degrees in the contact angle) [36].

Cell adhesion was further favored by coating the micro-channel surface with fibronectin. The combined effect of rugosity enhancement through micromachining and fibronectin coating significantly improved cell adhesion, thereby minimizing detachment under continuous flow.

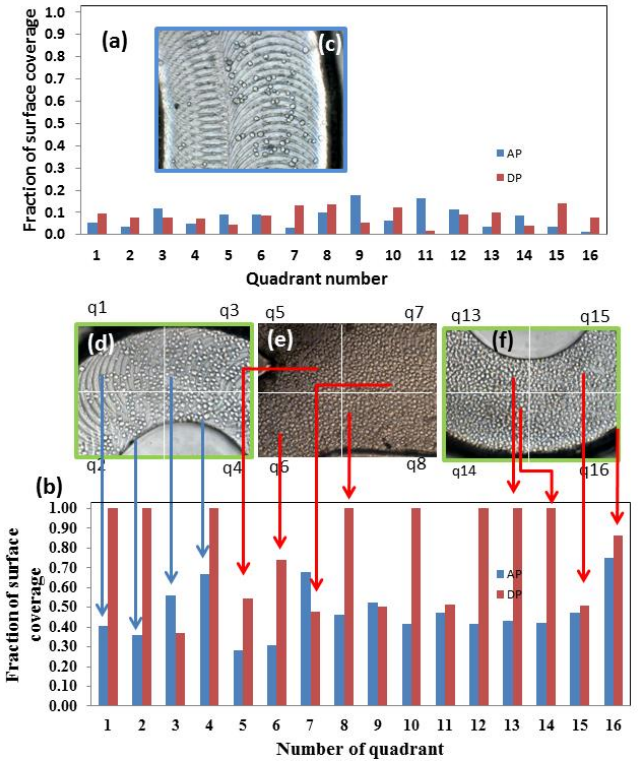

Figure 4. Cell proliferation on enhanced roughness surfaces, uncoated or coated with fibronectin, as measured in four images representative of different sections of a SD system. Each image was inspected using image analysis techniques to calculate the fraction of the surface containing cells anchored in each quadrant. Blue bars represent the fraction of area covered by cells after a period of incubation at static conditions (96 h). Red bars represent the area coverage in the same quadrants after 48 hours of continuous perfusion. In surfaces (a) not-coated with fibronectin, cell attachment is remarkably lower than in (b) surfaces coated. (c) Inset shows a representative quadrant of a system not-coated with fibronectin after perfusion. Optical microscopy images of a SD channel system coated with fibronectin are presented at (d) static conditions and (e) and (f) after 48 hours of continuous perfusion.

In Figure 4, we present evidence of the advantages of the fibronectin coating in terms of cell adhesion and proliferation. Optical microscopy images of different sections of all the micro-channel systems were divided in four quadrants and the extent of cell attachment was calculated, using image analysis, as the fraction of the surface occupied by cells. We found marked differences between the performance of surfaces (uncoated and coated with fibronectin) in terms of initial cell attachment and cell proliferation under continuous flow. The initial cell attachment was lower for untreated micro-device surfaces (Figure 4a) than for treated surfaces (Figure 4b). After 48 h of continuous flow, the fraction of surface occupied by cells was higher in the fibronectin coated channels than in the uncoated channels. Images of representative sections of the SD micro-device after static incubation (blue bars) and after continuous flow at 3μL min^{-1} (red bars) are presented in Figure 4. Figures 2e and 2f show electron microscope images of cells attached to micro-channel surfaces treated as previously described.

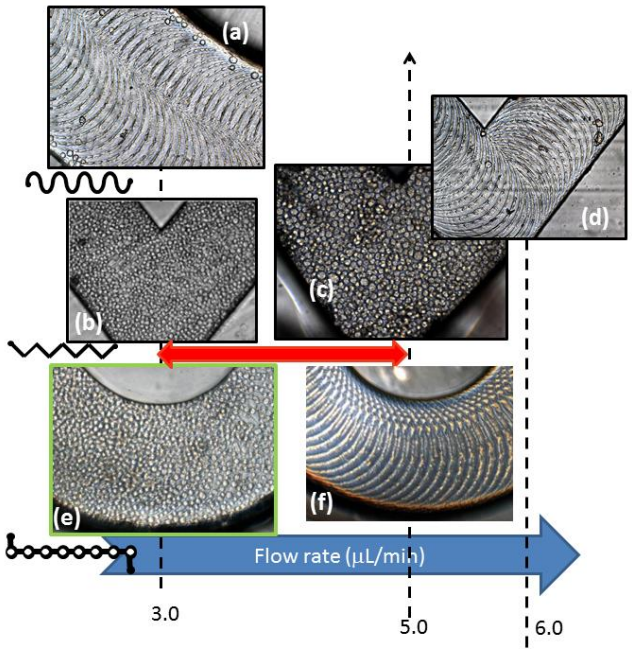

Figure 5. Cell proliferation in micro-devices at different flow rates (3, 5, and 6 μL min^{-1}). In wavy (WV) channels, (a) practically total cell detachment occurred at 3 μL min^{-1}. In zigzag (ZZ) channels, cell proliferation was observed at (b) 3 and (c) 5 μL min^{-1}, and cell detachment occurred at (d) 6 μL min^{-1}. In SD systems, cell proliferation was observed at (e) 3 μL min^{-1}, and (f) practically full cell detachment occurred at 5 μL min^{-1}.

Cells with a wide range of different diameters were observed (between 8 to 23 μm). The appearance of cell borders suggested strong attachment in a monolayer type arrangement. Figure 3c shows a confocal image of a single cell attached to the surface. These images indicated that the cells adopted a disc type shape, deviating from the characteristic spherical geometry observed in suspension cultures. Although surface texturizing significantly improved cell attachment, the geometry of the device ultimately determined the maximum flow rate that the system could withstand without significant cell detachment.

Geometry is determinant for cell attachment

Geometry has an important effect on cell attachment. Green et al. [38] studied cell attachment in micro-channels with straight, curved, and sharply turning shapes. The authors found, that the sharply turning micro-channels had low local velocity areas at the corners, where cell deposition and attachment were higher than that seen in curved or straight channels. In a previous communication, we also reported comparable results [30]. Here, we considered WV, ZZ, and SD micro-device configurations (Figure 1). Given the viscosity and density of the culture medium (an aqueous solution), the dimensions of the channel and the flow rates used originated laminar flows in the low Reynolds number range of $0.1<Re<0.8$. In concept, low Re numbers will favor appropriate renewal of nutrients, while minimizing cell detachment. In DS micro-devices, adequate cell proliferation occurred at 3 μL min^{-1}, but significant cell detachment was observed at 5 μL min^{-1} (Figure 5).

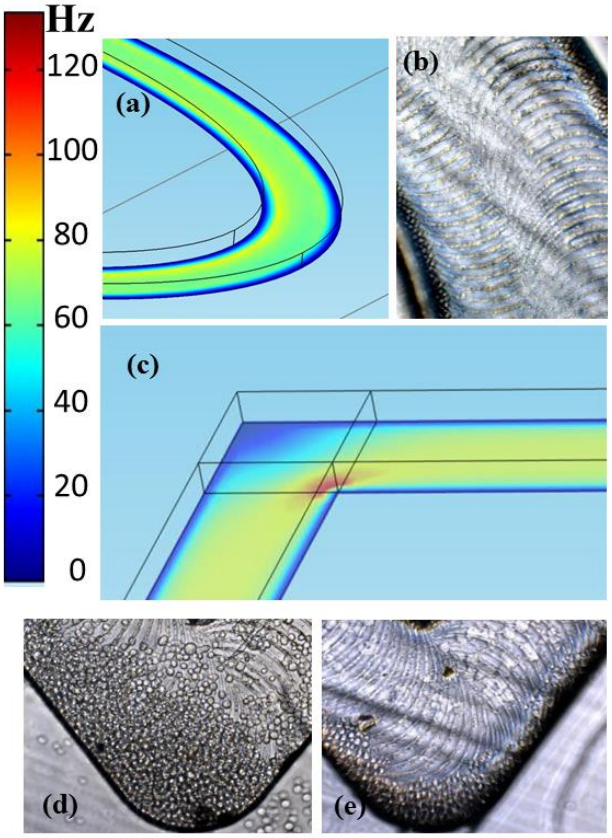

Figure 6. Relationship between vorticity and cell detachment. (a) The vorticity field at the bottom surface of a wavy (WV) channel. (b) In WV systems, cell detachment occurs at 3 µL min^{-1}, and cells at the walls are the last to be detached. (c) Vorticity field at the bottom surface of zigzag (ZZ) channels. Cell detachment occurs at 6 µL min^{-1}; cell attached to low vorticity zones (d, e) are the last to be detached.

In micro-fluidic systems, cell detachment is clearly associated with fluid velocity gradients at the surface of attachment (*i.e.*, shear stresses, vorticities) [39-42]. However, even at these low Re laminar flows, important differences in the fluid mechanics conditions were imposed by geometry. The geometry of the channel system was crucial for determining the maximum operational flow of the system that would also avoid significant cell detachment. In WV channels, almost complete cell detachment occurred at flow rates of 3 µL min^{-1}, while the threshold flow for complete cell detachment was 6 µL min^{-1} in ZZ systems.

Our results suggest that fluid dynamics and mass transfer aspects determine the degree of attachment and proliferation in the different geometries studies. We further investigated the relationship between cell attachment and fluid dynamics in our systems by using CFD to determine the distribution of local velocities, shear stresses, and vorticities [43]. Figure 6a and 6c shows a comparison of the vorticity distributions at a flow rate condition of 3 µL min^{-1}, as calculated by CFD at the bottom surface, for the WV and ZZ micro-channels. The presence of more extensive areas of low local vorticity at the bottom surface of our devices favored cell attachment.

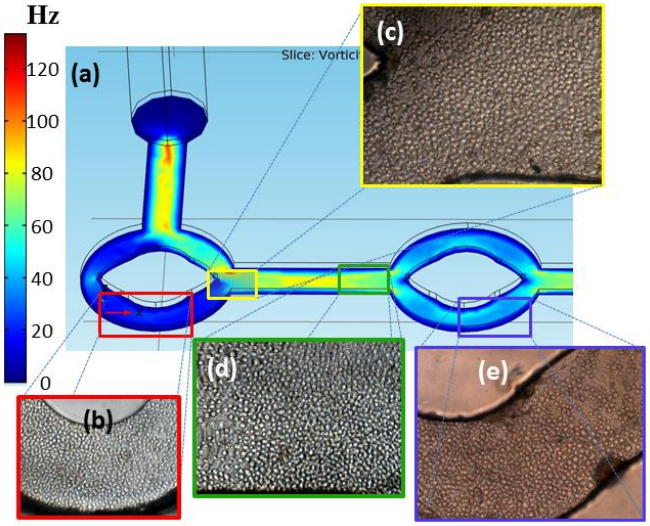

Figure 7. Vorticity and cell proliferation in SD channels. (a) The vorticity field at the bottom surface of a SD system. Cell proliferation at different sections of a SD system: (b) in the first donut-shaped element, (c) at the entrance of a convergent flow straight section, (d) at the outlet of a straight section, and (e) in a portion of the second donut shape element. Areas of higher cell proliferation correlate to low vorticity zones.

The flow condition of at 3µL min^{-1} caused extensive cell detachment in the WV system, while the ZZ system showed confluent cell cultures that could be sustained for several days. In the WV system, the simplest geometry originates a simple flow field; a parabolic laminar flow with the maximum local velocity (v_{max}) of 2.27 mm s^{-1} at the center line of the channel. Note that the distribution of vorticities at the bottom of the surface – that is, the "lifting" that anchored cells experience – exhibits lower values only in the neighborhood of the wall. Consistently, in continuous flow experiments, those regions are where cells remained attached (Figure 6b).

The flow in the ZZ channel exhibited a more complex structure (Figure 6c). As expected, the areas with the lowest local velocity were aligned with the channel walls. However, additional zones of relatively low vorticity existed in the corners. In these low local vorticity (and shear) zones, cell attachment to the micro-channel surface appeared to be stronger, since the cells were able to withstand higher flow rates for longer times before detachment (Figure 6d and 6e).

The SD micro-device was the most complex geometry that we studied. The rationale of the SD design was that it would resemble a series of micro-tanks connected within each other through micro-channels. It consisted of 8 oval reservoirs (2 mm diameter) with a cylindrical post at the center; the ovals were connected to each other through micro-channels (1.1 mm long, 0.4 mm wide). Evidently, this more convoluted geometry resulted in a more complex flow field (Figure 7a). For instance, the distribution of local vorticities and velocities was more heterogeneous in the SD device than in the ZZ micro-channel. In the SD system, v_{max}=3.00 mm s^{-1}, located at the center line of the narrow channel segments, was the second lowest among the three systems.

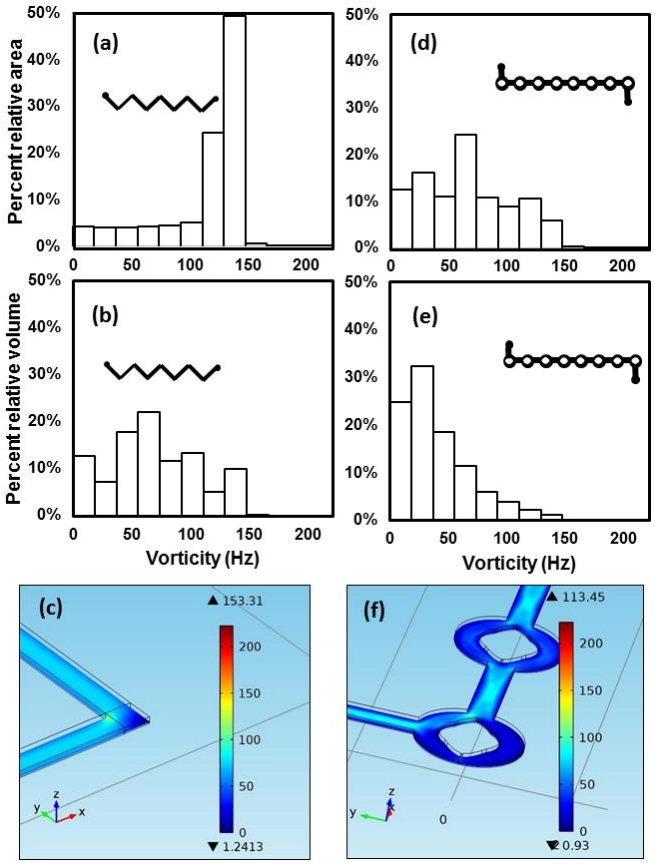

Figure 8. Distribution of vorticity values in a zigzag system (ZZ) operated at 5 μL min^{-1} at (a) the bottom surface, and (b) the entire system volume, and (c) vorticity field at the system horizontal mid-plane. Distribution of vorticity values in a serial donut system (SD) operated at 5 μL min^{-1} at (a) the bottom surface, and (b) the entire system volume, and (c) vorticity field at the system horizontal mid-plane.

Note that, in the region of each "donut," the SD design practically doubles the cross-sectional area of the flow, yielding a more extensive area of low to medium flow. With this simple variation in the geometry, we intended to provide areas of low shear/low vorticity that would lead to stronger cell attachment and increased residence time per unit of length of the chip. Indeed, cells initially and preferably anchored at the bottom of the cylindrical reservoirs, in the low vorticity areas, as opposed to the straight micro-channels between them, where highest vorticity values prevailed (Figure 7c and 7d). Our observations are consistent with previous reports of higher cell attachment in low vorticity areas (or conversely, higher cell detachment in high vorticity zones) [38,39].

At 3 μL min^{-1}, the more suitable conditions for cell attachment provided by the more extensive areas of low vorticity at the bottom surface of the ZZ and SD micro-channels explain the tolerance of the ZZ and SD systems to continuous flow (Figure 6 and 7). However, this argument cannot explain why, at 5 μL min^{-1}, cell proliferation is only observed in ZZ channels. At this flow condition, the distribution of vorticities appears to be even more suitable for cell attachment on the SD surfaces than on the ZZ surfaces. Indeed, CFD simulations show that the fraction of surface area available for cell attachment with vorticity values below 50 Hz is more extensive in SD systems than in ZZ systems (Figure 8a,d). One possible explanation may be O_2 availability: Mehta et al. [44] solved the equations of convective and diffusive O_2 transport for a monolayer of cells in a micro-channel covered by a PDMS lid. The authors showed that at high cell density and moderate flow rates, local oxygen concentrations at the cell monolayer may become growth limiting. We speculate that, at 5 μL min^{-1}, the diffusive/convective O_2 transport from the lid of the SD system may be insufficient to support the demand of the cells attached to the bottom surface. Our CFD results show that the field of vorticities values across the entire volume is more evenly distributed in ZZ systems, with similar volumetric fractions of low, medium, and high vorticity (Fifure 8b,c,e,f). This more homogeneous distribution could lead to more effective mixing and more adequate mass transfer conditions in the ZZ system.

Cell proliferation and mAb production

Our laminar continuous micro-devices established practically a "plug flow." Functionally, these systems behaved like continuous tubular reactors, where a balance between attached cell proliferation and cell detachment determined the cell density at any given point in the system. The flow rate determined the availability of nutrients and the removal of the product of interest (mAb) and other metabolic products (*i.e.*, lactic acid). Slow flow rates would be expected to minimize cell detachment, but might not favor adequate oxygen mass transfer (from the top surface of the device). On the other hand, excessively high flow rates might cause detachment rates to exceed cell proliferation.

As we have demonstrated, cell detachment strongly depended on the geometry of the device. Therefore, we expected to observe different mAb production in micro-devices with different geometries, even at the same flow rate. As a first and simple approximation, the mAb concentration at the outlet of the device should be determined by the number of viable and functional cells attached to the surface. However, different flow conditions might induce different metabolic states in the attached cells. Therefore, the possibility existed for observing different specific cell productivities under different flow rate conditions.

For the three geometries, an approximately similar cell density was achieved after four days of static culture. In the ZZ arrays, we observed confluent cell attachment at flow conditions of 3 and 5 μL min^{-1}. However, in the SD system, we only observed confluent growth at 3 μL min^{-1}; cell detachment and negligible mAb production were observed in SD channels at 5 μL min^{-1}. Figure 5 summarizes our observations relative to attached cell proliferation.

We determined mAb production in the ZZ and SD systems at continuous flow rate conditions of 3 and 5 μL min^{-1}. For these experiments, the concentration of functional antibody (that recognizes αTNF) was determined by ELISA from samples collected at the outlet of the device. Measurements were taken at different times during the period of continuous operation (Figure 9a). In general, in ZZ and SD micro-channels, we observed an increasing outlet mAb concentration profile during the first 48 hours of operation. This suggests that cell proliferation is actively occurring during continuous feeding.

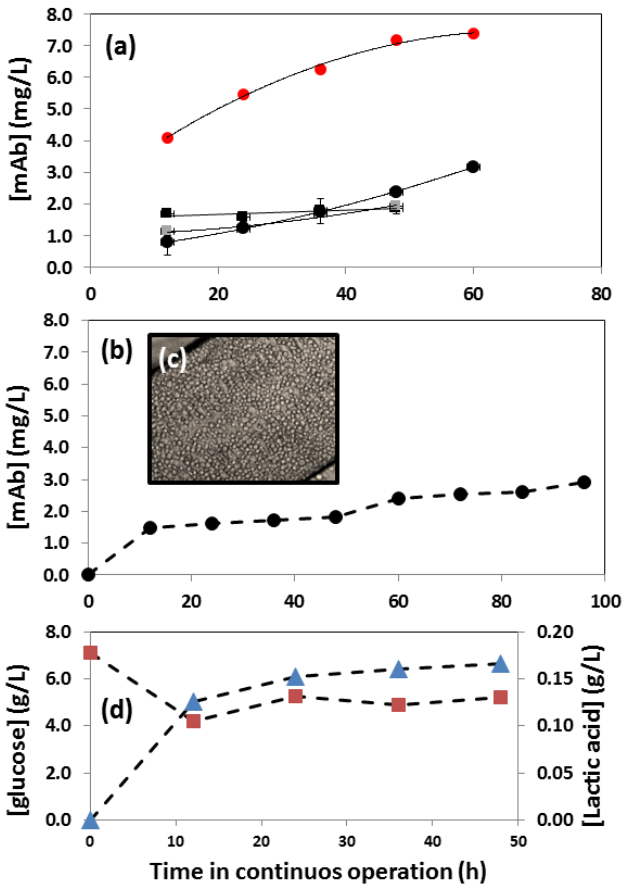

Figure 9. (a) Monoclonal antibody (mAb) concentration at the outlet of perfusion micro-devices at different times of continuous operation: (a) ZZ micro-channel operated at 3 µL min^{-1} (■), and 5 µL min^{-1} and (■), SD system operated at 3 µL min^{-1} at regular (●) and (d) high cell density (●). (b) mAb concentration profile in time in an experiment of 100 h of continuous perfusion at 3 µL min^{-1}(●) in a ZZ channel. (c) Attached cells exhibited viabilities above 97%. (d) Concentration profiles of glucose (■) and lactic acid (▲).

During this time period, at similar initial seeding (attached cell concentrations at the end of the static culture period), a similar concentration profile was observed in the ZZ and SD systems operated at 3 µL min^{-1}. However, after 48 hours, the outlet mAb concentration appears to increase more rapidly in SD than in ZZ micro-devices.

We conducted additional experiments in the SD systems at higher seeding densities (HSD). The SD systems have geometrical features that allow for high initial cell densities (*i.e.*, more area per unit of length due to their donut-shaped design). This low vorticity surface is suitable for cell attachment and sustained proliferation. In these experiments, we observed outlet steady-state concentrations of 7 mg L^{-1} after 60 hours of continuous operation (Figure 9a).

Envisioning the future use of perfusion micro-chips for pilot (or commercial) production of biopharmaceuticals, one concern is their robustness and stability for extended periods of operation. Although most of our experiments were aimed at studying the transient behavior after the onset of continuous operation (first 60 hours), our observations suggest that long–term, continuous operation of these devices is feasible. However, the dynamics of these systems is complex, and a steady state is not achievable in short time frames. Figure 9b shows the outlet mAb concentration in a ZZ channel over a period of 100 h. For this experiment, the device was previously inoculated and maintained under static incubation for 96 hours. During the first 40 hours of continuous operation, the mAb concentration increased to approximately 1.75 mg L^{-1} and appeared to reach a first plateau. Later, the concentration increased again to reach an apparent steady state at a value of 2.0 mg L^{-1}. If the outlet concentration of mAb is assumed to be approximately proportional to the concentration of viable anchored cells, these experiments indicate that two sequential stages of cell proliferation occurred in this particular experiment. In geometries where the entire surface of the device was not necessarily equally favorable for colonization (*i.e.*, different regions experience different vorticities), the occurrence of several sequential cell proliferation stages is feasible. Indeed, in the case of the SD device, we did not observe complete cell confluence after the first 60 hours of continuous operation (see Figure 7).

An additional indicator of the feasibility of extended operation is the observed cell viability. We conducted viability assays on the population of cells attached to the surface of devices after continuous operation of 48 and 60 hours and observed viabilities above 96%, as estimated by routinely used techniques (*e.g.*, trypan blue assay) (Figure 9d). These observations suggest that the cell layer is effectively and constantly renewing; apoptotic cells are probably being detached as metabolically active cells proliferate on the available surface.

We also evaluated the concentration profiles of glucose (the substrate) and lactic acid (one of the main CHO metabolic by-products) during continuous operation in a ZZ micro-channel operated at 5 µL min^{-1}, the fastest flow rate and lowest residence time condition that we explored. Remarkably, glucose conversion reached a value of 25% for a residence time of less than a minute (Figure 8d). The concentration of lactic acid reached a plateau after 30 hours of operation and was then maintained at low levels (under 0.20 g L^{-1}). Future studies will consider longer channel lengths and operational periods.

Given the dimensions of each device, different liquid volumes can be contained on them, and consequently, different residence times can be obtained at the same flow rate (Table 2).

Table 2. Residence time, final mAb concentration, and productivities for zigzag (ZZ) and serial donuts (SD) micro-devices operated in static mode (flow rate=0) and continuous mode (at different flow rates). For comparison, data from fed-batch runs in a fully instrumented fed-batch stirred tank reactor are included (FSTR).

Flow rate (µL min^{-1})	Volume (µl)	RT (min)	[mAb] mg L^{-1}	Productivity mg mL^{-1} min^{-1}
0	2.6276 (µl)	5760	9.269 ± 0.480	0.0016
3	2.6276 (µl)	0.88	1.931 ± 0.147	2.2046
5	2.6276 (µl)	0.53	1.860 ± 0.256	3.5394
0	2.4504 (µl)	5760	7.234 ± 0.192	0.0013
3	2.4504 (µl)	0.82	3.170 ± 0.022	3.8810
3@HSD*	2.4504 (µl)	0.82	7.360 ± 0.142	9.0107
0	1.5000 (L)	25200	203.5 ± 43.13	0.0080

*Experiments conducted at high seeding densities

We should expect a higher overall number of cells and a higher antibody titer at the end of the devices with longer residence time. The calculation of specific quantities, such as productivity (mg of mAb per unit of volume per unit of time) or average cell concentration (cells/mm^2 or cells mL^{-1}), allows a direct and fair comparison among the devices. Table 2 compares residence times, outlet mAb concentrations, and productivities for the different bioreactor systems tested. After 96 hours of batch culture (static conditions), the mAb concentration in the micro-devices was between 7 and 10 mg L^{-1}. The highest concentration achieved in continuous micro-devices, in the SD systems, was in this range (7.360 ± 0.142 mg L^{-1}). Remarkably, the residence times in all our continuous experiments range between 0.53 and 0.58 min. Therefore, when the variable of time is considered, the productivity observed in the micro-device systems is three orders of magnitude higher when operated in continuous mode than in static culture. For the sake of comparison, in Table 2 we included data from fed-batch culture experiments in fully instrumented stirred tank reactors (1.5 L of volume). For these experiments, the culture protocol included several additions of feed B, as described in the Materials and methods, and a total culture time of 17 days. The productivity in continuous micro-devices was at least 3.0 orders of magnitude higher than in fed-batch bioreactors. In suspended culture fed-batch systems, the maximum cell density observed was 6.25+/-1.58 x10^6 cell mL^{-1}. In micro-devices, typical cell concentrations in confluent systems, as determined by image analysis, were 2.72 X10^6 cell cm^2 (equivalent to 68.06 x10^6 cell mL^{-1}). Therefore, the higher cell density in micro-devices (one order of magnitude) can only partially explain the dramatic increase in productivity achieved in continuous micro-devices. We speculate that the constant renewal of nutrients and the continuous removal of metabolic by-products (including lactic acid and CO_2), plays a key role in the enhancement of productivity of continuously fed micro-devices.

Conclusions

We cultured attached recombinant CHO cells, producers of a mAb, in three different channel micro-device geometries (WV, ZZ, and SD) and two different flow rates (3 and 5 µL min^{-1}). The surfaces of these channels were micro-machined to impart texture and coated with fibronectin to further favor CHO cell attachment. We found that both the geometry of the system and the flow rate determined the performance of these cell culture micro-devices in terms of cell proliferation and mAb production. CFD simulations revealed significant differences in the distribution of local vorticities among the three micro-device geometries studied here. In turn, these differences in the vorticity field resulted in important differences in cell adhesion and cell proliferation. In summary, in WV channel systems, practically full cell detachment occurred after 24 hours of continuous flow at a flow rate of 3 µL min^{-1}. In contrast, under flow rate conditions of 3 and 5 µL min^{-1}, ZZ systems maintained adequate cell proliferation and were able to withstand flow rates of 5 µL min^{-1}. On the other hand, almost complete cell detachment was observed in SD systems under those conditions. The mAb production correlated with cell proliferation: In ZZ and SD micro-devices, we observed outlet mAb concentrations in the range of 2 to 8 mg L^{-1}, with residence times of less than a minute and with maximum productivities of 9 mg mL^{-1} min^{-1}. These productivities are about three orders of magnitude higher than those typically reported in fed batch suspension cultures. Our results suggest that these continuous bio-pharma chips could be used for screening applications and inclusive piloting of biopharmaceuticals.

Acknowledgements

The authors acknowledge the financial support of Tecnológico de Monterrey (research seed fund CAT-122), and Laboratorios Landsteiner Scientific, México. We thankfully acknowledge CONACyT (Consejo Nacional de Ciencia y Tecnología) for the doctoral scholarship granted to LGG.

Notes and references

[a] *Tecnológico de Monterrey at Monterrey, Centro de Biotecnología-FEMSA*
[b] *Tecnológico de Monterrey at Monterrey, Departamento de Ingeniería Eléctrica y Computacional,*
[c] *Tecnológico de Monterrey at Monterrey, Centro de Innovación en Diseño y Tecnología,*
[*] *Tecnológico de Monterrey at Monterrey, Centro de Biotecnología-FEMSA, Ave. Eugenio Garza-Sada 2501, Monterrey, N.L., México. Fax: +52 8183284136; Tel: +52 8183582000; E-mail: Mario.alvarez@itesm.mx.*

† Electronic Supplementary Information (ESI) available: [details of any supplementary information available should be included here]. See DOI: 10.1039/b000000x/.

.

1 M. Krishan. Top Ten/Twenty Drugs 2011. *Knol Publishing*, 2012. Available: http://top10drugs.wordpress.com/2012/03/. Accessed 25 June 2012.
2 IMARC. Global Biopharmaceutical Market Report & Forecast (2012-2017). *International Market Analysis Research & Consulting*, 2012. Available: http://www.imarcgroup.com/global-pharmaceutical-market-report-forecast-2012-2017/. Accessed 25 June 2012.
3 P. A. Marichal-Gallardo and M. M. Alvarez, *Biotechnol. Prog.*, 2012, **28**, 899-916.
4 D.S. Dimitrov, 2012, *Methods Mol. Bio.*, 899:1-26.
5 J.M. Reichert, *mAbs* 2012 4(3):413-415.
6 Z. –N. Xia, X.-T- Cai, and P. Cao, *Yaoxue Xuebao*, 2012, **47**(10) 1275-1280.
7 A. Gilbert, K. McElearney, R. Kshirsagar, M.S. Sinacore and T. Ryll, *Biotechnol. Progr., 2013*, DOI: 10.1002/btpr.1787.
8 R. Kshirsagar, K. Mcelearney and A. Gilbert, *Biotechnol. Bioeng.*, 2012, **109**, 2523-2532.
9 A. Hilal-Alnaqbi, A.Y.C. Hu, Z. Zhang and M. Al-Rubeai, *Biotechnol. Bioeng*., 2013, **60**, 436-445.
10 K. P. Jayapal, K. F. Wlaschin, W-Sh. Hu and M. G. S. Yap, *Chem. Eng, Prog.*, 2007, **10**, 40-47.
11 J.Y. Kim, Y-G. Kim and G.M. Lee. *Appl. Microbiol. Biotechnol.*, 2012, **93**, 917–930.
12 V. Warikoo, R. Godawat, K. Brower, S. Jain, D. Cummings, E. Simons, T. Johnson, J. Walther, M. Yu, B. Wright, J. McLarty, K. P. Karey, C. Hwang, W. Zhou, F. Riske and K. Konstatinov, *Biotechnol. Bioeng*., 2012, **109**, 3018-3029.
13 S. F. Abu-Absi, L. Yang, P. Thompson, C. Jiang, S. Kandula, B. Schilling and A. A. Shukla, *Biotechnol. Bioeng.*, 2010, **106**, 894-905.
14 H. E. Abaci, R. Devendra, Q. Smith, S. Gerecht and G. Drazer, *Biomed. Microdevices*, 2012, **14**, 145-152.
15 B.J. Kim, T. Zhao, L. Young and P. Zhou. *Biotechnol. Bioeng.*, 2012, **109**, 137-145.
16 E. W. K. Young and D. J. Beebe, *Chem. Soc. Rev.*, 2010, **39**, 1036-1048.

17 K. Saadin, J.M. Burke, N.P. Patel, R.E. Zubajlo and I.M. White. *Biomed. Microdevices*, 2013, **15**, 645-655.

18 K.-J. Jang, A.P. Mehr, G.A. Hamilton, L.A. McPartlin, S. Chung, K.-Y. Suh, and D.E. Ingber, *Integ. Biol. (United Kingdom)*, 2013, **5**, 1119-1129.

19 S. Selimović, M.R. Dokmeci and A. Khademhosseini. *Curr. Opin. Pharmacol.*, 2013, In press.

20 N. Bose, T. Das, D. Chakraborty, T. K. Maiti and S. Chakraborty, *Lab Chip*, 2012, **12**, 69-73.

21 J.W. Hong, S. Song and J.H. Shin, *Lab Chip*, 2013, **13**, 3033–3040.

22 D. Huh, B. D. Mathews, A. Mammoto, M. Montoya-Zavala, H. Yuan Hsin and D. E. Ingber, *Science*, 2010, **328**, 1662-1668.

23 V.N. Goral, Ch. Zhou, F. Lai and P.K. Yuen, *Lab Chip*, 2013, **13**: 1039-1043.

24 B. Zhang, C. Peticone, S.K. Murthy, and M. Radisic. Biomicrofluidics, 2013, 7, 044125.

25 L.M. Li, W. Wang, S.H. Zhang, S.J. Chen, S.S. Guo, O. Français, J.K. Cheng and W.H. Huang, *Anal. Chem*., 2012, **83**, 9524-9530.

26 Ch. Liu, L. Wang, Z. Xu, J. Li, X. Ding, O. Wong and L. Chunyu, *J. Micromech. Microeng.*, 2012, **22**, art. no. 065008.

27 H.J. Kim, D. Huh, G. Hamilton G. and D.E. Ingber, *Lab Chip*, 2012, **12**, 2165-2174.

28 K.R. Love, T.J. Politano, V. Panagiotou, B. Jiang, T.A. Stadheim and J.C. Love, *PLoS ONE*, 2012, **7**, e37915. doi:10.1371

29 L. Kim, Y. C. Toh, J. Voldman and H. Yu, *Lab Chip*, 2007, **7**, 681-694.

30 L.D. Garza-García, L.M. Carrillo-Cocom, D. Araiz-Hernández, P. Soto-Vázquez, J. López-Meza, E.J. Tapia-Mejía, S. Camacho-León, E. García-López, C.A. Rodríguez-González and M.M. Alvarez, *Lab Chip*, 2013, **13**, 1243-1246.

31 E. Berthier, E. W. K. Young and D. Beebe, *Lab Chip*, 2012, **12**, 1224-1237.

32 A. Alrifaiy, O. A. Lindahl and K. Ramser, *Polymers*, 2012, **4**, 1349-1398.

33 I. Voiculescu, F. Li, ,X. Zhang, L.M. Cancel, J.M. Tarbell and A. Khademhosseini, *Sensors and Actuators, B: Chemical*, 2013, **182**, 696-705.

34 I. J. González-Leal, L. M Carrillo-Cocom, A. Ramírez-Medrano, F. López-Pacheco, D. Bulnes-Abundis, Y. Webb-Vargas and M.M. Alvarez, *Biotechnol. Prog.*, 2011, **27**, 1709-1717.

35 E. Vázquez, C.A. Rodríguez, A. Elías-Zuñiga and J. Ciurana, *Int. J. Adv. Manuf. Technol.*, 2010, **51**, 945-955.

36 K.J. Kubiak, M.C.T. Wilson, T.G. Mathia, Ph. Carval, *Wear*, 2011, **271**, 523-528.

37 D.G. Waugh, J. Lawrence, *Optics and Lasers in Engineering*, 2010, **48**, 707-715.

38 J.V. Green, T. Kniazeva, M. Abedi, D.S. Sokhey, M.E. Taslim and S.K. Murthy, *Lab Chip*, 2009, **9**, 677-685.

39 I. Rizvi, U. A. Gurkan, S. Tasoglu, N. Alagica, J. P. Celli, L. B. Mensah, Z. Mai, U. Demirci and T. Hasan, *PNAS*, 2013, **110**, E1974-E1983.

40 F.A. Bonilla, N. Kleinfelter, and J.H. Cushman, *Advances in Water Resources 2012, 30(6-7):1680-1695*.

41 C. Verdier, C. Couzon, and A. Duperray, *Eur. Biophys. J.*, 2009, **38**, 1035-1047.

42 L.S.L. Cheung, X. Zheng, A. Stopa, J.C. Baygents, R. Guzman, J.A. Schroeder, R.L. Heimark and Y. Zohar, *Lab Chip*, 2009, **9**, 1721-1731.

43 M.Y. Rotenberg, E. Ruvinov, A. Armoza and S. Cohen, *Lab Chip*, 2012, **12**, 2696-2703.

44 G. Mehta, K. Metha, D. Sud, J.W. Song, T. Bersano-Begey, N. Futai, Y.S. Heo, M-A. Mycek, J.J. Linderman and S. Takayama. *Biomed. Microdevices*, 2007, **9**, 123-134.

